

THE STABILITY OF MAGNETIZED ROTATING PLASMAS WITH SUPERTHERMAL FIELDS

MARTIN E. PESSAH^{1,2} and DIMITRIOS PSALTIS^{2,1}

ABSTRACT

During the last decade it has become evident that the magnetorotational instability is at the heart of the enhanced angular momentum transport in weakly magnetized accretion disks around neutron stars and black holes. In this paper, we investigate the local linear stability of differentially rotating, magnetized flows and the evolution of the magnetorotational instability beyond the weak-field limit. We show that, when superthermal toroidal fields are considered, both compressibility and magnetic tension terms, related to the curvature of toroidal field lines, should be taken fully into account. We demonstrate that, contrary to the results of most previous investigations, the presence of a toroidal component in the magnetic field plays a crucial role not only in the growth rates of the unstable modes but also in determining which modes are subject to instabilities. We find that, for rotationally supported configurations, the magnetorotational instability is stabilized at low wavenumbers for toroidal Alfvén speeds exceeding the geometric mean of the sound speed and the rotational speed. For a broad range of magnetic field strengths, we also find that two additional distinct instabilities are present; they both appear as the result of coupling between the modes that become the Alfvén and the slow modes in the limit of no rotation. We finally discuss the implication of our results for the validity of shearing box simulations in which superthermal toroidal fields are generated.

Subject headings: accretion, accretion disks — MHD — instabilities — plasmas

1. INTRODUCTION

Linear mode analyses provide a useful tool in gaining important insight on the relevant physical processes determining the stability of magnetized accretion flows. Previous studies of local linear modes of accretion disks threaded by weak magnetic fields have pointed out important clues on viable mechanisms for angular momentum transport and the subsequent accretion of matter onto the central objects (Balbus & Hawley 1991, 1998, 2002; Sano & Miyama 1999; Balbus 2003). They have also provided simplified physical models and analogies over which more complex physics can, in principle, be added (Balbus & Hawley 1992, 1998; Quataert, Dorland, & Hammet 2002). These treatments, mostly carried out in the MHD limit, invoked a number of approximations appropriate for the study of the evolution of short wavelength perturbations in the presence of weak fields. In this context, the strength of the magnetic field, B , is inferred by comparison of the thermal pressure, P , with the magnetic pressure, and is characterized by the parameter, $\beta = 8\pi P/B^2$.

It is not hard to find situations of astrophysical interest, however, in which the condition of weak magnetic fields is not satisfied. A common example is the innermost region of an accretion disk around a magnetic neutron star. It is widely accepted that X-ray pulsars are powered by accretion of matter onto the polar caps of magnetic neutron

¹Astronomy Department, University of Arizona, 933 N. Cherry Ave., Tucson, AZ, 85721; mpessah@as.arizona.edu

²Physics Department, University of Arizona, 1118 E. 4th St., Tucson, AZ, 85721; dpsaltis@physics.arizona.edu

stars. For this to occur, matter in the nearly Keplerian accretion disk has to be funneled along the field lines. This suggests that, at some radius, centrifugal forces and thermal pressure have to be overcome by magnetic stresses, leading naturally to regions where $\beta \lesssim 1$.

In the context of accretion disks, the presence of superthermal fields in rarefied coronae also seems hard to avoid, if coronal heating is a direct consequence of the internal dynamics of the disk itself rather than being produced by external irradiation from the central object. Three-dimensional MHD simulations by Miller & Stone (2000) showed that magnetic turbulence can effectively couple with buoyancy to transport the magnetic energy produced by the magnetorotational instability (MRI) in weakly magnetized disks to create a strongly magnetized corona within a few scale heights. On long time scales, the average vertical disk structure consists of a weakly magnetized ($\beta \simeq 50$) turbulent core below ~ 2 scale heights and a strongly magnetized ($\beta \lesssim 0.1$) non-turbulent corona above it. The late stages of evolution in these models show that the disks themselves become magnetically dominated. Machida, Hayashi, & Matsumoto (2000) also found that the average plasma β in disk coronae is $\simeq 0.1 - 1$ and the volume filling factor for regions with $\beta \lesssim 0.3$ is up to 0.1. Even in the absence of an initial toroidal component, simulations carried out by Kudoh, Matsumoto, & Shibata (2002) showed that low- β regions develop near the equator of the disk because of a strong toroidal component of the magnetic field generated by shear. On more theoretical grounds, strong toroidal magnetic fields produced by strong shear in the boundary layer region have been suggested as responsible for the observed bipolar outflows in young stellar objects (Pringle 1989). More recently, Pariev, Blackman, & Boldyrev (2003) found self-consistent solutions for thin magnetically-supported accretion disks and pointed out the necessity of assessing the stability properties of such configurations.

As a last example of astrophysical interest in which magnetic fields seem to play an important dynamical role in rotating fluid configurations, we cite magnetically supported molecular clouds. Observations of both large Zeeman line-splitting and of broad molecular lines support superthermal fields (see Myers & Goodman 1988 for further references and Bourke & Goodman 2003 for a review on the current understanding on the role of magnetic fields in molecular clouds). Values of the plasma β of the order of 0.1 – 0.01 have also been used in numerical studies of the structural properties of giant molecular clouds (Ostriker, Stone, & Gammie 2001).

In this paper we investigate the linear stability of differentially rotating flows without imposing any restrictions on the strength of the magnetic field. We do, however, restrict our attention to rotationally supported flows. In order to achieve this, we relax the Boussinesq approximation (see also Papaloizou & Szuszkiewicz 1992 and Blaes & Balbus 1994), which is valid only when the toroidal component of the field is subthermal (Balbus & Hawley 1991). Moreover, even though we perform a local analysis, we do consider curvature terms when evaluating magnetic forces, for they become important in the strong-field regime (see also Knobloch 1992). In most early studies of single-fluid MHD flows, it was found that the only effect of a toroidal field component is to quench the growth rates of the unstable modes already present in the standard MRI (Balbus & Hawley 1991; Blaes & Balbus 1994; see also Quataert, Dorland, & Hammet 2002). Here, we show that, when strong fields are considered and the above approximations are relaxed, the presence of a toroidal component of the magnetic field plays a crucial role not only in the growth rates of the unstable modes but also in determining which modes are subject to instabilities.³ As expected, the presence of a toroidal component breaks the symmetry of the problem, also giving rise to traveling modes. Moreover, for a broad range in magnetic field strengths, we find that two different instabilities are present. They both appear as the result of coupling between the modes that become the Alfvén and the slow mode in the limit of no rotation.

The paper is organized as follows. In §2, we describe the physical setup to be studied, present the dispersion relation to be solved, and discuss the importance of curvature terms in the limit of superthermal fields. In §3, we

³We will comment later in more detail on the paper by Curry & Pudritz (1995) who outlined the effects of a dynamically important toroidal field (in the case of an incompressible MHD flow) and address the similitudes and differences with our findings.

solve numerically the dispersion relation in some interesting regimes. In §4, we study the onset of instabilities as a function of magnetic field strengths and present some useful approximate criteria that enable us to study analytically some aspects of the full problem. In §5, we compare our results with previous investigations and discuss some of the implications of this study. Finally, in §6, we present a brief summary and our conclusions.

2. MHD EQUATIONS FOR PERTURBATIONS AND THE DISPERSION RELATION

We start with the set of equations that govern the behavior of a polytropic fluid in the MHD approximation,

$$\frac{\partial \rho}{\partial t} + \nabla \cdot (\rho \mathbf{v}) = 0, \quad (1)$$

$$\rho \frac{\partial \mathbf{v}}{\partial t} + (\rho \mathbf{v} \cdot \nabla) \mathbf{v} = -\rho \nabla \Phi - \nabla \left(P + \frac{\mathbf{B}^2}{8\pi} \right) + \left(\frac{\mathbf{B}}{4\pi} \cdot \nabla \right) \mathbf{B}, \quad (2)$$

$$\frac{\partial \mathbf{B}}{\partial t} + (\nabla \cdot \mathbf{v}) \mathbf{B} - (\mathbf{B} \cdot \nabla) \mathbf{v} + (\mathbf{v} \cdot \nabla) \mathbf{B} = 0, \quad (3)$$

and

$$P = P_0 \left(\frac{\rho}{\rho_0} \right)^\Gamma. \quad (4)$$

In these equations, ρ is the mass density, \mathbf{v} the velocity, P the gas pressure, and Γ the polytropic index; \mathbf{B} is the magnetic field and Φ the gravitational potential. We assume an axisymmetric steady background with no vertical stratification characterized by a cylindrical rotational profile $\Omega = \Omega(r)$ and threaded by a background magnetic field of the form $\mathbf{B} = [0, B_\phi(r), B_z(r)]$. The effect of including a radial component in the field is to generate a linear growth in time of the toroidal component (Balbus & Hawley 1991) and, for the sake of simplicity, we do not take this into account here. In the present treatment, we neglect the self gravity of the fluid. In fact, Pariev, Blackman, & Boldyrev (2003) showed that magnetically dominated accretion disks have lower surface and volume densities for a fixed accretion rate. This suggests that these systems are lighter than standard disks and thus are not subject to self gravity instabilities. Furthermore, we do not consider the influence of gravity in the vertical direction. This is consistent with the earlier assumption of no vertical stratification.

Equations for the perturbations.— In order to derive the set of equations to perform the linear mode analysis, we expand in Fourier series all the perturbed Eulerian quantities in terms of plane waves propagating only in the vertical direction as $\delta f = \sum \delta f_k e^{i(kz - \omega t)}$; where δf denotes the perturbation in a particular quantity, δf_k the amplitude of the Fourier mode with wavenumber k , and ω the mode frequency. This approach to the local stability analysis is physically motivated (since vertical modes correspond to the most unstable modes in the well studied MRI) and more tractable mathematically. The resulting linear set is given by

$$-\omega \frac{\delta \rho}{\rho} - \frac{i}{r} (\epsilon_4 + \rho') \delta v_r + k \delta v_z = 0, \quad (5)$$

$$-i\omega \delta v_r - 2\Omega \delta v_\phi - ik \frac{B_z \delta B_r}{4\pi \rho} + \frac{\epsilon_1}{r} \frac{B_\phi \delta B_\phi}{2\pi \rho} + \frac{B'_z}{r} \frac{B_z \delta B_z}{4\pi \rho} - \frac{1}{r} \left[(\epsilon_2 + B'_\phi) \frac{B_\phi^2}{4\pi \rho} + B'_z \frac{B_z^2}{4\pi \rho} + \rho' c_s^2 \right] \frac{\delta \rho}{\rho} = 0, \quad (6)$$

$$-i\omega \delta v_\phi + \frac{\kappa^2}{2\Omega} \delta v_r - ik \frac{B_z \delta B_\phi}{4\pi \rho} - \frac{1}{r} (\epsilon_3 + B'_\phi) \frac{B_\phi \delta B_r}{4\pi \rho} = 0, \quad (7)$$

$$-i\omega\delta v_z + ik\frac{\delta P}{\rho} + ik\frac{B_\phi\delta B_\phi}{4\pi\rho} + \frac{B'_z}{r}\frac{B_z\delta B_r}{4\pi\rho} = 0, \quad (8)$$

$$i\omega\delta B_r + ikB_z\delta v_r = 0, \quad (9)$$

$$-i\omega\delta B_\phi - \left(\frac{d\Omega}{d\ln r} + B'_\phi \frac{\omega}{k} \frac{B_\phi}{B_z} \right) \delta B_r - ikB_z\delta v_\phi + ikB_\phi\delta v_z = 0, \quad (10)$$

$$i\omega\delta B_z - B_z(\epsilon_4 + B'_z) \frac{\delta v_r}{r} = 0, \quad (11)$$

$$\frac{\delta P}{P} = \Gamma \frac{\delta \rho}{\rho}, \quad (12)$$

where we have omitted the subscript k in all perturbed quantities and κ stands for the epicyclic frequency,

$$\kappa^2 = 2\Omega \left[2\Omega + \frac{d\Omega}{d\ln r} \right]. \quad (13)$$

The quantities ρ' , B'_ϕ , and B'_z stand for the logarithmic derivatives, with respect to the radial coordinate, of the density and the toroidal and vertical components of the magnetic field,

$$\rho' = \frac{d\ln \rho}{d\ln r}, \quad B'_\phi = \frac{d\ln B_\phi}{d\ln r}, \quad \text{and} \quad B'_z = \frac{d\ln B_z}{d\ln r}. \quad (14)$$

The terms proportional to ϵ_1 and ϵ_2 in equation (6) and the term proportional to ϵ_3 in equation (7) are due to the effects of magnetic tension and they appear naturally when a cylindrical coordinate system is adopted. The terms proportional to ϵ_4 in equations (5) and (11) are related to flux conservation in cylindrical coordinates. The factors ϵ_i , with $i = 1, 2, 3, 4$, are just convenient dummy variables that we introduce in order to help us keep track of these curvature terms throughout the analysis. Although the three terms labeled by ϵ_1 , ϵ_2 , and ϵ_3 share the same physical origin (i.e., magnetic tension introduced by the curvature of toroidal field lines), it is useful to be able to distinguish among them because the one labeled with ϵ_2 vanishes in the limit of an incompressible flow. Moreover, we will later show that the term proportional to ϵ_1 is negligible when superthermal toroidal fields are considered. We will also discuss under which conditions the terms proportional to ϵ_4 can be neglected.

In spite of being linear in the perturbed quantities, the terms proportional to ϵ_i have been neglected in previous local studies of the MRI because of their $1/r$ dependence (but see also Knobloch 1992). However, the terms proportional to ϵ_1 , ϵ_2 , and ϵ_3 are also proportional to the magnitude of the toroidal component of the field. As we will show below, in order not to impose a constraint on the magnitude of the toroidal Alfvén speed with respect to the sound speed, these terms must be taken into account. In fact, these are the terms that govern the stability of the fluid in the superthermal regime. When all the ϵ_i are set equal to zero, we recover the results of previous analyses where these terms were not considered (e.g., Blaes & Balbus 1994; Balbus & Hawley 1998), while when they are set equal to unity we obtain our full treatment. Note that equations (9) and (11) ensure $\nabla \cdot \delta \mathbf{B} = 0$ only when finite curvature is considered (i.e., $\epsilon_4 = 1$).

Dispersion relation.— We define dimensionless variables, at a given radius, by scaling all the frequencies with the local rotational frequency Ω and all speeds with the local circular velocity Ωr . We also define a dimensionless wavenumber by multiplying the physical wavenumber by the radial coordinate r . In brief, we write

$$\frac{\omega}{\Omega} \rightarrow \omega, \quad (15)$$

$$\frac{\kappa}{\Omega} \rightarrow \kappa, \quad (16)$$

$$kr \rightarrow k, \quad (17)$$

$$\frac{1}{\Omega r} \sqrt{\Gamma \frac{P}{\rho}} \rightarrow c_s , \quad (18)$$

$$\frac{1}{\Omega r} \frac{B_\phi}{\sqrt{4\pi\rho}} \rightarrow v_{A\phi} , \quad (19)$$

and

$$\frac{1}{\Omega r} \frac{B_z}{\sqrt{4\pi\rho}} \rightarrow v_{Az} , \quad (20)$$

where we have introduced the dimensionless counterparts of the sound speed and the Alfvén speeds associated with the toroidal and vertical components of the magnetic field. Hereafter, unless otherwise mentioned, whenever we refer to frequencies, speeds, or wavenumbers, we are referring to their dimensionless counterparts.

In order to seek for non-trivial solutions of the homogeneous system of linear equations (5)-(12) we set its determinant equal to zero. The resulting characteristic polynomial is of the form

$$\omega^6 + a_4\omega^4 + a_3\omega^3 + a_2\omega^2 + a_1\omega + a_0 = 0 . \quad (21)$$

where,

$$\begin{aligned} a_4 &= -\{k^2(c_s^2 + v_{A\phi}^2 + 2v_{Az}^2) + \kappa^2 + [(\epsilon_2 + B'_\phi)(\epsilon_4 + \rho') - 2\epsilon_1 B'_\phi] v_{A\phi}^2 + B'_z(\rho' - B'_z)v_{Az}^2 + \rho'(\epsilon_4 + \rho')\} \\ a_3 &= -(2\epsilon_1 + \epsilon_3) 2k v_{A\phi} v_{Az} \\ a_2 &= k^4 v_{Az}^2 (2c_s^2 + v_{A\phi}^2 + v_{Az}^2) + k^2 \left[\kappa^2(c_s^2 + v_{A\phi}^2) + (2\epsilon_1 + \rho')(\epsilon_4 + \rho' - B'_\phi) v_{A\phi}^2 c_s^2 \right. \\ &\quad \left. + [(\epsilon_2 + B'_\phi)(\epsilon_4 + \rho') - B'_\phi(\epsilon_2 + B'_\phi)] v_{A\phi}^4 + [(\epsilon_2 + B'_\phi)(\epsilon_4 + \rho') - 2\epsilon_1(\epsilon_3 + B'_\phi + B'_z)] v_{A\phi}^2 v_{Az}^2 \right. \\ &\quad \left. + 2 \frac{d \ln \Omega}{d \ln r} v_{Az}^2 + v_{Az}^2 \{[\rho'^2 + (\epsilon_4 + B'_z)(\rho' - B'_z)] c_s^2 + B'_z(\epsilon_2 + \rho' - B'_z)v_{A\phi}^2 + \rho' B'_z v_{Az}^2\} \right] \\ a_1 &= 2k^3 v_{A\phi} v_{Az} [c_s^2 (2\epsilon_1 + \epsilon_3 + \epsilon_4 + 2\rho') + v_{A\phi}^2 (\epsilon_2 + \epsilon_3 + 2B'_\phi)] \\ a_0 &= -k^4 c_s^2 v_{Az}^2 \left(k^2 v_{Az}^2 + 2 \frac{d \ln \Omega}{d \ln r} \right) + k^4 v_{Az}^2 \{ (2\epsilon_1 + \rho') (\epsilon_3 + B'_\phi) c_s^2 v_{A\phi}^2 + (\epsilon_2 + B'_\phi) (\epsilon_3 + B'_\phi) v_{A\phi}^4 \} \\ &\quad + k^4 v_{Az}^4 B'_z [(\epsilon_4 + B'_z - \rho') c_s^2 - B'_z v_{Az}^2 + (\epsilon_3 - \epsilon_2) v_{A\phi}^2] . \end{aligned} \quad (22)$$

The dispersion relation (22) is the most general dispersion relation under our current set of assumptions.

We solved numerically the dispersion relation (22) for typical values of Alfvén speeds of interest in this paper, i.e., $v_{Az} \lesssim c_s \lesssim v_{A\phi} < 1$. Under these circumstances, the results show that the mode structure is rather insensitive to the steepness of the background gradients of the density profile, ρ' , and of the vertical and toroidal components of the field, B'_z and B'_ϕ . This is not surprising given the fact that all logarithmic gradients add as terms of order unity to the various curvature terms proportional to ϵ_1 , ϵ_2 , ϵ_3 and ϵ_4 . As a single exception, for the case in which $B_\phi \propto r^{-1}$ (i.e., $B'_\phi = -1$), the most important effects due to the finite curvature of toroidal field lines are canceled out by the gradients in the toroidal field. This should not be so surprising since, in this case, the forces produced by gradients in magnetic pressure cancel out the ones produced by magnetic tension due to the curvature of toroidal field lines.

A parametric study of the general dispersion relation (22) is a rather formidable task. However, for the sake of simplicity and to avoid the parametric study from being too extensive, we focus our attention on the study of differentially rotating, axisymmetric MHD flows with locally negligible background gradients in the density and magnetic field. In the rest of the paper, we consider that the only background flow variable with a non-negligible local radial gradient is the angular velocity Ω and set $\rho' = B'_\phi = B'_z = 0$. Under these conditions the dispersion relation (22)

becomes

$$\begin{aligned}
 \omega^6 - & [k^2(c_s^2 + v_{A\phi}^2 + 2v_{Az}^2) + \kappa^2 + \epsilon_2\epsilon_4 v_{A\phi}^2]\omega^4 - (2\epsilon_1 + \epsilon_3)2kv_{A\phi}v_{Az}\omega^3 + \left\{ k^4v_{Az}^2(2c_s^2 + v_{A\phi}^2 + v_{Az}^2) \right. \\
 & + k^2 \left[\kappa^2(c_s^2 + v_{A\phi}^2) + 2\epsilon_1\epsilon_4 v_{A\phi}^2 c_s^2 + \epsilon_2\epsilon_4 v_{A\phi}^4 + 2\frac{d\ln\Omega}{d\ln r}v_{Az}^2 + (\epsilon_2\epsilon_4 - 2\epsilon_1\epsilon_3)v_{A\phi}^2 v_{Az}^2 \right] \left. \right\} \omega^2 \\
 & + 2k^3v_{A\phi}v_{Az} [c_s^2(2\epsilon_1 + \epsilon_3 + \epsilon_4) + v_{A\phi}^2(\epsilon_2 + \epsilon_3)]\omega \\
 & - k^4v_{Az}^2 \left(k^2c_s^2v_{Az}^2 + 2\frac{d\ln\Omega}{d\ln r}c_s^2 - 2\epsilon_1\epsilon_3 c_s^2 v_{A\phi}^2 - \epsilon_2\epsilon_3 v_{A\phi}^4 \right) = 0. \tag{23}
 \end{aligned}$$

We note a few important points about the dispersion relation (23). Once all the dimensionless variables have been properly defined, it is not evident that the magnetic-tension terms, proportional to ϵ_1 , ϵ_2 , and ϵ_3 , will have a negligible role in determining the eigenfrequencies ω . This is because the non-vanishing toroidal component of the magnetic field introduces odd powers in the dispersion relation and hence break its even symmetry. In fact, small modifications in the odd-power coefficients can and do have an important impact on the nature (real vs. complex) of the solutions. Of course, whenever a given complex root is a solution of the dispersion relation (23) so is its complex conjugate, for the dispersion relation still has real coefficients. As we will see in §3 and describe in further detail in §4, these curvature terms introduce further coupling between the radial and toroidal directions, which in turn result in a strong coupling between the Alfvén and the slow mode. Although the original linear system (5)-(12) related 8 variables, the characteristic polynomial is only of 6th degree. This is because of two reasons. First, equations (9) and (11) can be combined into a single relationship between δB_r and δB_z , which is independent of ω . Second, as in all previous treatments, the polytropic equation (12) relates perturbations in density and in pressure, in a frequency-independent way. The fact that the dispersion relation (23) is of 6th and not of 4th degree, contrary to many previous works, is because we are taking into account the effects of finite compressibility. This can be seen immediately by taking the limit $c_s \rightarrow \infty$.

Previous treatments.— There has been some discussion in the past about the importance of the curvature terms for the stability of magnetized Keplerian flows (Knobloch 1992; Gammie & Balbus 1994). In studies in which these terms were considered (Knobloch 1992; Dubrulle & Knobloch 1993), compressibility effects were neglected. On the other hand, there have also been treatments in which compressibility was addressed but the curvature terms were neglected (Blaes & Balbus 1994). Both types of studies provided arguments for and against the importance of these terms. Because of the generality of our treatment, in which both curvature terms and compressibility effects are fully taken into account, we are able to address this issue in §5.

As a check, we can take the appropriate limits in the general dispersion relation (23) to recover the dispersion relations derived by previous investigations. Setting $\epsilon_i = 0$, for $i = 1, 2, 3, 4$, we recover the dispersion relation of Blaes & Balbus (1994),

$$\begin{aligned}
 \omega^6 - & [k^2(c_s^2 + v_{A\phi}^2 + 2v_{Az}^2) + \kappa^2]\omega^4 \\
 & + \left\{ k^4v_{Az}^2(2c_s^2 + v_{A\phi}^2 + v_{Az}^2) + k^2 \left[\kappa^2(c_s^2 + v_{A\phi}^2) + 2\frac{d\ln\Omega}{d\ln r}v_{Az}^2 \right] \right\} \omega^2 \\
 & - k^4v_{Az}^2 c_s^2 \left(k^2v_{Az}^2 + 2\frac{d\ln\Omega}{d\ln r} \right) = 0. \tag{24}
 \end{aligned}$$

The stability criterion derived from this dispersion relation is not different from the one derived, within the Boussinesq approximation, by Balbus & Hawley (1991). All the perturbations with wavenumber smaller than the critical wavenumber k_{BH} are unstable with

$$k_{BH}^2 v_{Az}^2 = -2\frac{d\ln\Omega}{d\ln r}. \tag{25}$$

We should also note that, even in the incompressible limit, not all the terms proportional to ϵ_i in the dispersion relation (23) are negligible (of course, the ones proportional to ϵ_2 are). In the limit $c_s \rightarrow \infty$, we recover the dispersion relation obtained by Dubrulle & Knobloch (1993) as the local limit of the corresponding eigenvalue problem

$$\omega^4 - (\kappa^2 + 2k^2 v_{Az}^2 + 2\epsilon_1 \epsilon_4 v_{A\phi}^2) \omega^2 - 2kv_{A\phi} v_{Az} (2\epsilon_1 + \epsilon_3 + \epsilon_4) \omega + k^2 v_{Az}^2 \left(k^2 v_{Az}^2 + 2 \frac{d \ln \Omega}{d \ln r} - 2\epsilon_1 \epsilon_3 v_{A\phi}^2 \right) = 0, \quad (26)$$

where we have explicitly left the factors ϵ_i that should be considered as unity. Note that, in order to compare expression (26) with equation (37) appearing in Dubrulle & Knobloch (1993) we have considered the limit of negligible background gradients and assumed that the modes propagate only in the vertical direction.

When the toroidal magnetic field is negligible, i.e., when $v_{A\phi} \rightarrow 0$ in equation (26), we recover the dispersion relation for the incompressible MRI and the onset of unstable modes is still given by expression (25). For weak toroidal fields, i.e., $v_{A\phi} \ll 1$, we can read off the small corrections to the critical wavenumber from the constant coefficient,

$$k_{oi}^2 v_{Az}^2 = -2 \frac{d \ln \Omega}{d \ln r} + 2\epsilon_1 \epsilon_2 v_{A\phi}^2. \quad (27)$$

For stronger fields, however, the $\omega = 0$ mode is no longer unstable (see the Appendix for a general discussion about the stability of the $\omega = 0$ mode when compressibility and curvature terms are considered) and it is necessary to solve equation (26) in order to find the critical wavenumber for the onset of the instability. Roughly speaking, we would expect the solutions of equation (26) to depart significantly from the solutions to the incompressible version of (24) when $v_{A\phi}^2 \gtrsim |d \ln \Omega / d \ln r|$, or $v_{A\phi} \gtrsim 1.2$ for a Keplerian disk. Since we consider rotationally supported configurations (i.e., $v_{A\phi} \lesssim 1$) in this paper, we will not address the modifications to the mode structure caused by curvature terms in incompressible MHD flows.

It is important to stress that, for both dispersion relations (24) and (26), in the case of rotationally supported disks, the stability criterion is insensitive (or, at most, very weakly sensitive in the incompressible case) to the magnitude of the toroidal component of the field. As we will see throughout our study, the stability criteria that emerge from equation (23) are significantly different from the ones discussed in this section. We will also see that, the term proportional to ϵ_2 , which depends upon curvature and compressibility effects and is, therefore, absent from either equation (24) or (26), plays an important role in determining the mode structure in the general case.

3. NUMERICAL SOLUTIONS

We solved numerically the dispersion relation (23) for the frequency ω as a function of the wavenumber k , employing Laguerre's root finding method (Press et al. 1992). As a typical situation of interest, we consider a Keplerian disk with $c_s = 0.05$ and $v_{Az} = 0.01$. As it will be seen from the range of values of k in which the various instabilities occur, the case of quasi-toroidal superthermal fields is perfectly suited to be studied in the local approximation, $k \gg 1$, provided that $v_{Az} \ll 1$.

To better appreciate the effects that the curvature terms have on the stability of the modes, a set of solutions to the dispersion relation (23) is shown in Figures 1 and 2.⁴ Each of the three panels, in both figures, shows the real and imaginary parts of the solutions for different values of the toroidal field strength, parameterized by $v_{A\phi}$. The left panel shows the solutions to the full dispersion relation (23), i.e., when $\epsilon_1 = \epsilon_2 = \epsilon_3 = \epsilon_4 = 1$. The central panel shows the solutions to (23) when compressibility is neglected in the curvature terms, i.e., when $\epsilon_1 = \epsilon_3 = \epsilon_4 = 1$ and $\epsilon_2 = 0$.

⁴Some animations of the results presented in Figs. 1, 2, 7, and 8 are available at <http://www.physics.arizona.edu/~mpessah/research/>

For the sake of comparison, the right panel shows the solutions to the dispersion relation (24), in which all curvature terms are neglected.

We first analyze Figure 1. When all magnetic tension terms are neglected (right panel), the qualitative structure of the normal modes of the plasma is insensitive to the magnitude of the toroidal field component (see Blaes & Balbus 1994). However, the situation is very different when the magnetic tension terms are included. For weak toroidal fields, i.e., $v_{A\phi} \lesssim 0.1$, the solutions seem quite insensitive to the curvature terms; indeed these terms do not seem to play a significant role in altering the local stability properties of magnetized Keplerian flows compared to what is quoted elsewhere in the literature. As it will be seen later, for a Keplerian disk, the presence of the curvature terms is significant once $v_{A\phi}^2 \gtrsim c_s$, which in this case translates into $v_{A\phi} \gtrsim 0.22$.

For stronger toroidal fields, i.e., when $v_{A\phi} \gtrsim 0.2$, the modes with the longest wavelengths become stable when all curvature terms are included, in sharp contrast to the case in which $\epsilon_2 = 0$. For even stronger toroidal fields, i.e., when $v_{A\phi} \gtrsim 0.3$, a second instability appears at long wavelengths, while the original instability is suppressed. When $v_{A\phi} \gtrsim 0.4$, both instabilities coexist as separate entities and the original instability reaches smaller and smaller spatial scales, when the magnitude of the toroidal field increases. For even higher toroidal fields, i.e., when $v_{A\phi} \gtrsim 0.7$, the largest unstable wavenumber of the instability that developed for $v_{A\phi} \gtrsim 0.3$ approaches k_{BH} (see eq. [25]). The major implication of neglecting compressibility in the curvature terms is that the original instability seems to be totally suppressed for toroidal fields larger than the ones corresponding to $v_{A\phi} \gtrsim 0.3$.

As it is clear from the dispersion relation (23), the presence of the toroidal component in the field introduces odd powers of the mode frequency ω and hence breaks the symmetry between positive and negative real parts of the solutions. The physical meaning of this is clear. The phase velocities of the instabilities are no longer zero and they are propagating vertically throughout the disk. This, of course, is not the case for the unstable solutions to relation (24) regardless of the magnitude of $v_{A\phi}$. In that case, the most noticeable effect of an increasing toroidal field is to reduce the phase velocity of the stable modes beyond k_{BH} (which is itself independent of $v_{A\phi}$).

It is also interesting to analyze how the presence of the curvature terms modifies the growth rates of the unstable modes as a function of the toroidal magnetic field. This is shown in Figure 2. Again, there are no significant changes for $v_{A\phi} \lesssim 0.1$; however, quite significant modifications to the growth rates are present for $v_{A\phi} \gtrsim 0.2$. The sequence of plots in the left panel shows more clearly the suppression of the original instability, the appearance of the instability at low wavenumbers, the return of the instability at high wavenumbers, and finally the fusion of these last two. The right panel in this figure shows what has been so far thought as the only effect of a strong toroidal component, i.e., a reduction in the growth rate of the non-propagating unstable modes (see e.g., Blaes & Balbus 1994 and Gammie & Balbus 1994). When the curvature terms are considered fully, the effects are more dramatic. Note also that, the growth rate of the original instability is reduced faster from the first to the second plot in the left panel in Figure 2 with respect to their counterparts in the right panel of the same figure.

4. THE ONSET OF INSTABILITIES

4.1. Unstable Modes

In §3 we presented how the structure of the various modes evolves as a function of the toroidal field strength and noted that, for a range of field strengths, two different instabilities are clearly distinguishable. Here, we obtain the conditions (i.e., the range of wavenumbers and toroidal field strengths) for which unstable modes are present. We start by plotting in Figure 3 the range of unstable wavenumbers as a function of the toroidal field strength. As a reference, we have plotted the case for a Keplerian disk. The black dots in the diagram represent the unstable wavenumbers,

kv_{A_z}/c_s , for a given toroidal Alfvén speed, $v_{A\phi}/c_s$.

Three regions of unstable modes are clearly distinguishable. Region I represents the evolution of the original instability present in the topmost three plots in the left panel in Figure 1. This is the region where the MRI lives. Strictly speaking, the MRI is confined to the region where $v_{A\phi}/c_s \ll 1$. As we will comment in §4.2, instability I is no longer incompressible beyond this point. The maximum wavenumber for which this instability exists is independent of $v_{A\phi}$ and corresponds to the critical wavenumber for the onset of the MRI (i.e., k_{BH} in eq. [25]). The stabilization of the long-wavelength perturbations beyond a critical value of the toroidal Alfvén speed is also evident in this region. For larger toroidal fields, shorter and shorter wavelengths are stabilized up to the ones corresponding to k_{BH} .

Region II shows the evolution of the instability that is only present for wavenumbers $k > k_{BH}$. Note that k_{BH} is now the minimum wavenumber for the onset of instability II. In this case, increasing $v_{A\phi}/c_s$ gives rise to unstable modes with even shorter wavelengths. Finally, Region III shows the instability that appears for intermediate wavenumbers (see for example the third plot in the left panel in Figure 1). Note that the shortest unstable wavelength in this region approaches k_{BH} for large values of $v_{A\phi}/c_s$.

4.2. Analytic Approximations

In this section we obtain analytical approximations to dispersion relation (23) in various limits, which will help us identify the different critical curves in Figure 3.

Let us note that the fast (or magnetosonic) modes are reasonably well decoupled from the rest of the oscillations (see left panels in Fig.1). By studying the modes that satisfy the condition $\omega^2 \ll k^2 c_s^2$, we effectively eliminate the fast modes from our analysis. This can be done for strong toroidal fields because, even in the presence of rotation, the magnetosonic modes are well described by $\omega^2 \simeq k^2(c_s^2 + v_A^2)$. Note that imposing $\omega^2 \ll k^2 c_s^2$ is a distinct and weaker condition than asking for the MHD fluid to be incompressible ($c_s \rightarrow \infty$). By eliminating these fastest modes, it is possible to find a 4th degree dispersion relation in ω , whose solutions constitute a very good approximation to the interesting modes seen in Figures 1 and 2.

We first write the equations for the evolution of the perturbations in the magnetic field. For the sake of clarity, we present the intermediate steps with the appropriate physical dimensions. Substituting equations (5), (11), and (12) in (8), with $\rho' = B'_\phi = B'_z = 0$, we obtain δv_z in terms of δB_ϕ and δB_z ,

$$\delta v_z = -\frac{k\omega c_s^2}{(kc_s)^2 - \omega^2} \left[\frac{v_{A\phi}^2}{c_s^2} \frac{\delta B_\phi}{B_\phi} + \frac{\delta B_z}{B_z} \right]. \quad (28)$$

Using this result in equation (10) we find,

$$ikB_z \delta v_\phi = -\frac{d\Omega}{d \ln r} \delta B_r - i\omega \delta B_\phi - i\omega B_\phi \frac{(kc_s)^2}{(kc_s)^2 - \omega^2} \left[\frac{v_{A\phi}^2}{c_s^2} \frac{\delta B_\phi}{B_\phi} + \frac{\delta B_z}{B_z} \right]. \quad (29)$$

From equations (5), (11), and (28) we can recast $\delta \rho$ in terms of δB_ϕ and δB_z as

$$\frac{\delta \rho}{\rho} = -\frac{k^2 v_{A\phi}^2}{(kc_s)^2 - \omega^2} \frac{\delta B_\phi}{B_\phi} + \left[1 - \frac{(kc_s)^2}{(kc_s)^2 - \omega^2} \right] \frac{\delta B_z}{B_z}. \quad (30)$$

Finally, we can write equations (28)-(30) for the modes whose frequencies satisfy $\omega^2 \ll k^2 c_s^2$ as,

$$\delta v_z = \frac{\omega}{k} \left[\left(\frac{v_{A\phi}}{c_s} \right)^2 \frac{\delta B_\phi}{B_\phi} + i \frac{\epsilon_4}{kr} \frac{\delta B_r}{B_z} \right], \quad (31)$$

$$ikB_z\delta v_\phi = - \left[\frac{d\Omega}{d \ln r} - \frac{\epsilon_4 \omega}{r k} \frac{B_\phi}{B_z} \right] \delta B_r - \left[1 + \left(\frac{v_{A\phi}}{c_s} \right)^2 \right] i\omega \delta B_\phi, \quad (32)$$

and

$$\frac{\delta\rho}{\rho} = - \frac{v_{A\phi}^2}{c_s^2} \frac{\delta B_\phi}{B_\phi}, \quad (33)$$

where we have used equations (9) and (11) to recast δB_z in terms of δB_r . Note that, neglecting the factor ω^2 against $k^2 c_s^2$ in equation (31), and therefore in equations (29) and (30), effectively reduces to neglecting the term proportional to ω in equation (8). Thus, for the modes of interest, the condition $\omega^2 \ll k^2 c_s^2$ is a statement about force balance in the vertical direction, which is made explicit in equation (33). In this way, we can see how important variations in the density are, in the presence of strong toroidal fields (see also Balbus & Hawley 1991). For $v_{A\phi} \gg c_s$, even small variation in the toroidal component of the field can have an important impact in the dynamics of the perturbations. For this reason, the assumption of an incompressible MHD flow is not valid, whenever superthermal toroidal fields are considered. Note that, in order to recover the incompressible MRI in the limit $\epsilon_i \rightarrow 0$, for $i = 1, 2, 3, 4$, we have not neglected the factor unity against $(v_{A\phi}/c_s)^2$, in equation (32).

We now have all the elements to write equations (6) and (7) in terms of δB_r and δB_ϕ . Using equations (31)-(33), valid in the limit $\omega^2 \ll k^2 c_s^2$, we obtain, in dimensionless form,

$$\begin{aligned} -\omega^2 \delta B_r + 2i\omega \left[1 + \left(\frac{v_{A\phi}}{c_s} \right)^2 \right] \delta B_\phi = & - \left[2 \frac{d \ln \Omega}{d \ln r} + (kv_{Az})^2 - 2\epsilon_4 \frac{\omega}{k} \frac{v_{A\phi}}{v_{Az}} \right] \delta B_r \\ & - ikv_{A\phi}v_{Az} \left[2\epsilon_1 + \epsilon_2 \left(\frac{v_{A\phi}}{c_s} \right)^2 \right] \delta B_\phi, \end{aligned} \quad (34)$$

$$-\omega^2 \delta B_\phi \left[1 + \left(\frac{v_{A\phi}}{c_s} \right)^2 \right] - i\omega \left[2 + \epsilon_4 \frac{\omega}{k} \frac{v_{A\phi}}{v_{Az}} \right] \delta B_r = -(kv_{Az})^2 \delta B_\phi + ikv_{A\phi}v_{Az}\epsilon_3 \delta B_r. \quad (35)$$

These equations are the generalization of the set of equations used to illustrate the physics behind the MRI as a system of masses coupled by a spring in a differentially rotating background. Indeed, in the incompressible limit and neglecting the curvature terms proportional to ϵ_i , we recover the set of equations presented elsewhere (Balbus & Hawley 1992, 1998).

Setting the determinant of the linear system (34)-(35) equal to zero and taking the limit $v_{A\phi} \gg c_s$ provides the following approximate dispersion relation that is valid for strong toroidal fields,⁵

$$\omega^4 - (\kappa^2 + k^2 v_{Az}^2 + \epsilon_2 \epsilon_4 v_{A\phi}^2) \omega^2 - 2kv_{A\phi}v_{Az}(\epsilon_2 + \epsilon_3)\omega + k^2 v_{Az}^2 \left[\frac{c_s^2}{v_{A\phi}^2} \left(k^2 v_{Az}^2 + 2 \frac{d \ln \Omega}{d \ln r} \right) - \epsilon_2 \epsilon_3 v_{A\phi}^2 \right] = 0. \quad (36)$$

Note that we have not neglected the factor $c_s^2/v_{A\phi}^2$ in the last term in equation (36) because its contribution is non-negligible at large wavenumbers. The solutions to the dispersion relation (36), for a Keplerian disk with $v_{A\phi} = 0.45$, $c_s = 0.05$, and $v_{Az} = 0.01$, are shown in the central panels in Figure 4. For the sake of comparison, the left panels in the same figure show the solutions of the full dispersion relation (23).

Note that the term proportional to ϵ_1 is not present in (36). This feature has important consequences in understanding the physics behind the stability of strongly magnetized compressible flows. It has been suggested (Curry & Pudritz 1995) that the magnetic tension term $B_\phi \delta B_\phi / r$ (i.e., the one proportional to ϵ_1 in eq. [6]) is responsible for the

⁵Note that, had we taken the opposite limit, i.e., $c_s \gg v_{A\phi}$, we would have recovered the dispersion relation (26).

stabilization of long-wavelength perturbations via the restoring forces provided by toroidal field lines in strong fields. This argument sounds compelling, but even if this were the case, we can see from the last term in equation (34) that the term proportional to ϵ_1 is not dynamically important for $v_{A\phi} \gg c_s$. At least in the radial direction, it is rather the term proportional to ϵ_2 the one governing the deviation compared to the stability properties of weak toroidal fields. This is in complete agreement with equation (33).

The dispersion relation (36) is of the form

$$\omega^4 + b_2\omega^2 + b_1\omega + b_0 = 0. \quad (37)$$

For this 4th order equation to have complex roots (corresponding to unstable modes), its discriminant has to be negative, i.e.,

$$D_4(v_{A\phi}, kv_{Az}) = -4b_2^3b_1^2 - 27b_1^4 + 16b_0b_2^4 - 128b_2b_0^2 + 144b_2b_1^2b_0 + 256b_0^3 < 0. \quad (38)$$

The modes satisfying this condition are shown as black dots in Figure 5. This analytical criterion agrees well with the numerical results for most of the values of the parameter $(v_{A\phi}/c_s, kv_{Az}/c_s)$ with the exception of some of the unstable modes close to the separatrix of the Regions I and II, defined in §4.1.

Limiting wavenumbers for Regions I and II.— The modes satisfying the condition $D_4 = 0$ correspond to the limits of Regions I, II, and III in Figure 5. Their analytical expressions, however, are complicated. Yet, some more progress can be made by realizing that the solutions to the second order equation obtained by simply dropping the ω^4 term in equation (36),

$$(\kappa^2 + k^2v_{Az}^2 + \epsilon_2\epsilon_4v_{A\phi}^2)\omega^2 + 2kv_{A\phi}v_{Az}(\epsilon_2 + \epsilon_3)\omega - k^2v_{Az}^2 \left[\frac{c_s^2}{v_{A\phi}^2} \left(k^2v_{Az}^2 + 2\frac{d\ln\Omega}{d\ln r} \right) - \epsilon_2\epsilon_3v_{A\phi}^2 \right] = 0, \quad (39)$$

constitute a very good approximation to the solutions of the dispersion relation (23) whenever the frequency of the modes satisfies $\omega^2 \ll 1$. This can be appreciated by comparing the left and right panels in Figure 4. The physics behind this approximation is not as direct as the physics behind the condition $\omega^2 \ll k^2c_s^2$, but it can also be understood in terms of force balance, this time in the radial direction. The dispersion relation (39) can be obtained by neglecting the term proportional to ω^2 in equation (34), setting to zero the determinant of the resulting linear system given by (34)-(35) and taking the limit $v_{A\phi} \gg c_s$. This approximation is equivalent to neglecting the term proportional to ω in equation (6) and hence related to neglecting the radial acceleration experienced by a displaced fluid element.

Setting the discriminant of equation (39) to zero, gives an equation in k with solutions that are the limiting wavenumbers for the onset of instabilities I and II in Figure 5, i.e.,

$$\begin{aligned} D_2(v_{A\phi}, kv_{Az}) = (kv_{Az})^4 &+ \left[\kappa^2 + 2\frac{d\ln\Omega}{d\ln r} - v_{A\phi}^2 \left(\frac{v_{A\phi}^2}{c_s^2} - \epsilon_4 \frac{c_s^2}{v_{A\phi}^2} \right) \right] (kv_{Az})^2 \\ &+ 2\frac{d\ln\Omega}{d\ln r} \left[\kappa^2 - v_{A\phi}^2 \left(\frac{v_{A\phi}^2}{c_s^2} - \epsilon_4 \frac{c_s^2}{v_{A\phi}^2} \right) \right] - \epsilon_4 v_{A\phi}^4 = 0. \end{aligned} \quad (40)$$

Here, we have set $\epsilon_2 = \epsilon_3 = 1$ but have explicitly left ϵ_4 to show that its contribution to the onset of instabilities I and II is not important when $v_{A\phi} \gg c_s$, as long as we are considering a rotationally supported disk. We mention, however, that the numerical solutions show that the contribution of the term proportional to ϵ_4 is small but not negligible for the unstable modes in region III. Neglecting the terms proportional to ϵ_4 , the solutions to equation (40) are simply

$$(kv_{Az})_{1,2}^2 = \frac{1}{2} \left[\frac{v_{A\phi}^4}{c_s^2} - \left(\kappa^2 + 2\frac{d\ln\Omega}{d\ln r} \right) \right] \pm \frac{1}{2} \left| \frac{v_{A\phi}^4}{c_s^2} - 4 \right|. \quad (41)$$

One of this solutions coincides always with k_{BH} (eq. [25]),

$$(k_{c1}v_{\text{Az}})^2 = -2 \frac{d \ln \Omega}{d \ln r}, \quad (42)$$

and the other one is

$$(k_{c2}v_{\text{Az}})^2 = \frac{v_{\text{A}\phi}^4}{c_s^2} - \kappa^2. \quad (43)$$

The modes with wavenumbers in the range $[\min(k_{c1}, k_{c2}), \max(k_{c1}, k_{c2})]$ are unstable. In Figure 5, the critical curves $k_{c1}(v_{\text{A}\phi})$ and $k_{c2}(v_{\text{A}\phi})$ are shown, with the proper normalization, as dashed lines. The critical wavenumber k_{c2} in equation (43) will be positive only for toroidal Alfvén speeds larger than

$$v_{\text{A}\phi}^{cI} = \sqrt{\kappa c_s}. \quad (44)$$

This is the critical value of the Alfvén speed beyond which the modes with longest wavelength, in Region I (see Fig. 5), begin to be stable. For a Keplerian disk, the epicyclic frequency coincides with the orbital frequency and thus, in dimensionless units, $\kappa^2 = 1$. In this case, the critical Alfvén speed for k_{c2} to be positive corresponds to $v_{\text{A}\phi} = 0.223$. This is the reason for which the long-wavelength modes are already stable in the second plot in the left panel in Figure 1, where $v_{\text{A}\phi} = 0.25$.

Incidentally, we find that the values of toroidal Alfvén speeds for which the standard MRI gives the appropriate range of unstable modes are not as restricted to $v_{\text{A}\phi} \ll c_s$ but rather to $v_{\text{A}\phi} \ll \sqrt{\kappa c_s}$. For $v_{\text{A}\phi} \gtrsim \sqrt{\kappa c_s}$, the standard MRI is stabilized at low wavenumbers. We point out that, Papaloizou & Szuszkiewicz (1992), by means of a global stability analysis of a compressible flow, found that for a slim disk threaded only by a vertical field, the flow is stable if the vertical Alfvén speed exceeds, within a factor of order unity, the geometrical mean of the sound speed and the rotational speed. In dimensionless units, this stability criterion translates into $v_{\text{A}z} \gtrsim \sqrt{c_s}$.

The limiting case in which $k_{c1} = k_{c2}$, is reached for

$$v_{\text{A}\phi}^{cII} = \sqrt{2c_s}. \quad (45)$$

Note that for $c_s = 0.05$, this corresponds to a value for the critical toroidal Alfvén speed of $v_{\text{A}\phi} = 0.316$. This situation is to be compared with the mode structure in the third plot in the left panel in Figure 1, where $v_{\text{A}\phi} = 0.32$.

Limiting wavenumbers for Region III.— In the previous section we presented some useful analytical approximations to describe the dependence of the critical values of the toroidal Alfvén speeds and wavenumbers defining Regions I and II on the different quantities characterizing the MHD flow. We could not, however, find simple analytical expressions to describe satisfactorily the corresponding behavior of the critical values defining Region III. We will describe qualitatively how the different regions of instability in Figure 3 depend upon the magnitude of the sound speed and the steepness of the rotation profile in the next section.

5. DISCUSSION

In this section, we address several issues related to the importance of the curvature terms in determining the stability criteria obeyed by the solutions to the dispersion relation (23). We comment on some controversies raised by previous investigations that have treated the standard MRI taking into account, in various ways, either compressibility or curvature of the background flow. We also highlight the similarities and differences of our findings with the results of Curry & Pudritz (1995), who also found the emergence of a new (but different) instability for strong toroidal fields in the case of an incompressible MHD flow. Finally, we address potential implications for shearing box models of neglecting magnetic tension terms induced by the curvature of the background fields.

5.1. Importance of curvature terms

In section §2 we mentioned that the terms proportional to ϵ_i , for $i = 1, 2, 3, 4$, are usually neglected due to their $1/r$ dependence. Some of these terms, however, are also proportional to the magnitude of the toroidal field. In this paper, we found that, when strong toroidal fields are considered, these terms produce substantial modifications to the stability criterion found to be held in the limit of weak fields. After solving the full problem, we are in a better position to understand why this is the case.

To illustrate the point, consider the ratio of the third term to the term proportional to ϵ_2 in equation (6) and the ratio of the third term to the term proportional to ϵ_3 in equation (7), i.e.,

$$R_1 = \frac{\epsilon_2}{ik} \frac{B_\phi^2}{\rho B_z} \frac{\delta\rho}{\delta B_r} \quad \text{and} \quad R_2 = \frac{\epsilon_3}{ik} \frac{B_\phi}{B_z} \frac{\delta B_r}{\delta B_\phi}. \quad (46)$$

In order to ensure that the contributions due to curvature are negligible in a local analysis, regardless of the magnitude of the toroidal field component, we should be able to ensure that the conditions $R_1 \ll 1$ and $R_2 \ll 1$ hold in the limit of large k for any value of $v_{A\phi} \lesssim 1$. While it is encouraging that both dimensionless ratios are proportional to $1/k$, they are also proportional to the ratio of perturbed quantities, which we do not know *a priori*. It is only *after* having found the eigenfrequencies $\omega(k)$ by taking into account *all* the curvature terms that we can properly address this issue.

We can calculate the dependence of the ratios R_1 and R_2 as a function of the wavenumber as follows. The ratio R_1 can be recast using equations (33) and (34) as

$$R_1 = \frac{\epsilon_2 v_{A\phi}}{k v_{Az}} \left(\frac{v_{A\phi}}{c_s} \right)^2 \frac{\omega^2 - \left(2 \frac{d \ln \Omega}{d \ln r} + k^2 v_{Az}^2 - 2\epsilon_4 \frac{\omega}{k} \frac{v_{A\phi}}{v_{Az}} \right)}{2\omega \left[1 + \left(\frac{v_{A\phi}}{c_s} \right)^2 \right] + k v_{Az} v_{A\phi} \left[2\epsilon_1 + \epsilon_2 \left(\frac{v_{A\phi}}{c_s} \right)^2 \right]}. \quad (47)$$

In a similar way, we can rewrite the ratio R_2 using equation (35). We obtain,

$$R_2 = \frac{\epsilon_3 v_{A\phi}}{k v_{Az} \omega} \frac{\omega^2 \left[1 + \left(\frac{v_{A\phi}}{c_s} \right)^2 \right] - k^2 v_{Az}^2}{\omega \left[2 + \epsilon_4 \frac{\omega}{k} \frac{v_{A\phi}}{v_{Az}} \right] + \epsilon_3 k v_{Az} v_{A\phi}}. \quad (48)$$

For the sake of simplicity, let us consider a given value for the toroidal Alfvén speed, e.g., $v_{A\phi} = 0.4$. Figure 6 shows the dependence of the ratios R_1 and R_2 for the unstable modes on wavenumber. The eigenfrequencies $\omega(k)$ for the unstable modes were obtained by solving equation (23) with $\epsilon_i = 1$, for $i = 1, 2, 3, 4$, considering a Keplerian disk with $c_s = 0.05$ and $v_{Az} = 0.01$. The ratios R_1 and R_2 for the unstable modes (with $v_{A\phi} = 8c_s$) in regions II and III in Figure 3 are clearly identified. The complete mode structure corresponding to this case can be seen in the plot with $v_{A\phi} = 0.4$ in the left panel of Figure 1.

It is important to stress that neither the real nor the imaginary parts of either R_1 or R_2 are negligible compared to unity even for Alfvén speeds of order a few times the sound speed. In fact, for the unstable modes, the ratio R_1 is of order unity and the ratio R_2 is in some cases larger by one order of magnitude. Their functional form is significantly different than the assumed $1/k$.

5.2. Magneto rotational Instabilities with superthermal fields

In §3 we demonstrated that, when the toroidal magnetic field in a differentially rotating MHD flow becomes superthermal, three distinct instabilities can be identified, which we denote by roman numerals I, II, and III in Figure 3. The qualitative characteristics of these instabilities are summarized below.

In contrast to the traditional MRI, all three instabilities correspond to compressible MHD modes. Moreover, while the traditional MRI corresponds to perturbations with negligible displacements along the vertical direction, these is not true for any of the three instabilities with superthermal toroidal fields. Instead, vertical displacements are an important characteristic of these instabilities and they occur with negligible acceleration, under a force balance between thermal and magnetic pressure. Finally, as in the case of the MRI, there is no significant acceleration along the radial direction but rather a force balance between magnetic tension, magnetic pressure, and thermal pressure.

In Figures 7 and 8 we study numerically the sensitivity of the three instabilities on the properties of the background flow. As also shown in the case of the traditional MRI (Balbus & Hawley, 1991), instability I occurs only in differentially rotating flows, with an angular velocity that is a decreasing function of radius. However, instability I also requires the presence of a non-negligible thermal pressure. Either a radially increasing angular velocity or a superthermal toroidal field can suppress instability I and hence the traditional MRI.

Instability II is ubiquitous, whenever the background toroidal field of the flow is significantly superthermal. Indeed, it occurs even for flat (see Fig. 7) or very cold (see Fig. 8) flows. In a sense opposite to instability I, the steepness of the rotational profile determines the minimum unstable wavenumber, whereas the magnitude of the sound speed determines the minimum toroidal field strength required for the instability to occur.

Finally, instability III depends strongly on the rotational profile but very weakly on the sound speed. For rotationally supported flows (i.e., for $v_{A\phi} \ll 1$), instability III occurs only for significantly steep rotational profiles, e.g., for $q \gtrsim 1.0$ for the parameters depicted in Figure 7.

5.3. Comparison to previous analytical studies

Soon after the original paper by Balbus & Hawley (1991), Knobloch (1992) critiqued their approach to the study of local instabilities, among other things, for lacking the contributions of curvature terms. He formulated the stability analysis of a vertical, unstratified, incompressible disk as an eigenvalue problem in the radial coordinate. He found that the presence of a toroidal field component changes the conditions for the presence of the instability as well as the character of the unstable modes from purely exponentials to overstable (i.e., $Re[\omega] \neq 0$). Gammie & Balbus (1994) argued against Knobloch's findings regarding overstability, stating that it arose as a consequence of having kept only small order terms (like v_A/c_s and $v_A/\Omega r$). They concluded that these contributions would have been negligible had the flow been considered compressible.

As we comment in §4.2, Knobloch's dispersion relation is correct even in the limit $c_s \gg v_{A\phi}$ (i.e., without the necessity of imposing strict incompressibility). Formally speaking, the linear term in ω in equation (26) does break the symmetry of the problem allowing for unstable modes with $Re(\omega) \neq 0$. But it is also the case that in the limit $c_s \gg v_{A\phi}$, because of the relative magnitude of the coefficients in the dispersion relation (26), we do not expect the stability properties of the flow to differ greatly from those described by the incompressible MRI. As we mention in the introduction, in order to see significant differences, the Alfvén speed would have to be of the order of the circular speed and therefore we do not expect the curvature terms to play a significant role on the stability of incompressible, rotationally supported flows.

On the other hand, if we allow the MHD fluid to be compressible and consider the curvature of the background flow, the mode structure can be radically different from what is expected for the compressible MRI (c.f. Blaes & Balbus 1994). This is the case, even if the toroidal Alfvén speed exceeds the sound speed by a factor of a few without the necessity of violating the condition of a rotationally supported disk (see Fig. 1).

Blaes & Balbus (1994) considered the stability of axisymmetric perturbations in weakly ionized and weakly mag-

netized shear flows. They showed that strong toroidal fields can fully stabilize the flow, when ionization equilibrium is considered in the two-fluid approach. As part of their study, they relaxed the Boussinesq approximation in the case of a single fluid and argued that, to all orders in field strength, B_ϕ does not affect the stability criterion. As also noted by Curry & Pudritz (1995), this conclusion was drawn consistently with neglecting the curvature terms.

Curvature terms cannot, of course, be neglected in global treatments of magnetized accretion disks. Then, it is not surprising that new instabilities, distinct from the MRI, have already been found in global studies in which strong fields were considered. In particular, Curry & Pudritz (1995) performed a global stability analysis to linear axisymmetric perturbations of an incompressible, differentially rotating fluid, threaded by vertical and toroidal fields. They consider power-law radial profiles for the angular velocity and the toroidal and vertical components of the field. Each of these were parameterized as $\Omega \propto r^{-a}$, $B_\phi \propto r^{-b+1}$, and $B_z \propto r^{-c+1}$, respectively. Most of their analysis dealt with a constant vertical field and they allowed variations of the exponents (a, b) , with the restriction that they correspond to a physical equilibrium state with a stationary pressure distribution. Although the majority of the paper dealt with global characteristics, they also performed a WKB analysis and conclude that, for $3/2 \leq a = b \leq 2$ and $v_{A\phi} < 1$, the growth rate of unstable modes is suppressed on both short and long wavelengths and it approaches zero when $v_{A\phi} \rightarrow 1$. On the other hand, for $a = b \neq 2$ and $v_{A\phi} > 1$, they found a new instability, with a growth rate that increased with $v_{A\phi}$. They call this the Large Field Instability (LFI) and showed that it can be stabilized for sufficiently large v_{Az} .

It is worth mentioning the major qualitative differences between the LFI and the new instability discussed in §3 that emerges for $k < k_{BH}$ after the stabilization of the MRI. Although it is true that, for our instability to be present, it is necessary for the toroidal Alfvén speed to exceed the local sound speed, there is no need to invoke Alfvén speeds larger than the local rotational speed. This is in sharp contrast with the LFI which only appears for $v_{A\phi} > 1$. Regarding the range of unstable wavenumbers, the LFI remains unstable for $k \rightarrow 0$, albeit with diminishing growth rate for large values of v_{Az} . This is not the case for the new instability present at low wavenumbers in our study. This can be seen, for example, in the fourth plot in the left panel in Figure 1. Perhaps the most noticeable difference is that the two instabilities in Curry & Pudritz (1995) that are present in the case $a = b \neq 2$ do not seem to coexist under any particular circumstances. The instability present for $v_{A\phi} < 1$ reaches zero growth for $v_{A\phi} \rightarrow 1$, while the LFI appears for $v_{A\phi} = 1$ and its growth rate is proportional to $v_{A\phi}$. When compressibility is considered, however, the two new instabilities found in our study can coexist even for Alfvén speeds smaller than the local rotational speed.

5.4. Implications for shearing box simulations

In an attempt to capture the most relevant physics without all the complexities involved in global simulations, the shearing box approach has been widely used in numerical studies of magnetic accretion disks (see, e.g., Hawley, Gammie, & Balbus 1994). The aim of the shearing box approximation is to mimic a small region of a larger disk. The size of the box is usually $H_z \times 2\pi H_z \times H_z$, with H_z the thermal scale height of the isothermal disk. In this approach, it is common to adopt a pseudo-Cartesian local system centered at R_o and in corotation with the disk with an angular frequency Ω_o , with coordinates $x = R - R_o$, $y = R_o(\phi - \Omega_o t)$, and z . The effects of differential rotation are then considered by imposing a velocity gradient in the radial direction. For a Keplerian accretion disk this is achieved by setting $v_y = -(3/2)\Omega_o x$.

In most studies of unstratified shearing boxes, Alfvén speeds rarely exceed the value of the local sound speed (see, e.g., Hawley, Gammie, & Balbus 1995, 1996). This is mainly because they are designed to simulate the midplane of the disk where the flow is relatively dense. In §4.2, we have seen that, as long as the toroidal Alfvén speed does not exceed the critical value $v_{A\phi}^2 = c_s \kappa$, neglecting magnetic tension due to curvature of toroidal field lines does not seem to affect the outcome of the MRI and hence the shearing box approach is well justified. However, when stratification is

taken into account, usually by adopting a density profile of the form $\rho = \rho_o \exp[-z^2/(2H^2)]$ in the case of isothermal disks, the steep drop in the density beyond a few scale heights can potentially lead to a magnetically dominated flow with Alfvén speeds larger than the critical value $v_{A\phi}^2 = \kappa c_s$.

As discussed in the introduction, Miller & Stone (2000) carried out 3D MHD simulations to study the evolution of a vertically stratified, isothermal, compressible, magnetized shear-flow. The simulations were local in the plane of the disk but vertically extended up to ± 5 thermal scale heights. This allowed them to follow the highly coupled dynamics of the weakly magnetized disk core and the rarefied magnetically-dominated (i.e., $\beta < 1$) corona that formed above the disk, for several (10 to 50) orbital periods.

They considered a variety of models, all sharing the same initial physical background, but different initial field configurations. In particular, they considered the following values: $\Omega = 10^{-3}$, $2c_s^2 = 10^{-6}$ (so that $H_z = \sqrt{2}c_s/\Omega = 1$), and $R = 100$. We mention some of the results they obtained for the models with initial toroidal fields (BY), which were qualitatively similar to the zero net z -field (ZNZ) models. After a few orbital periods, the presence of a highly magnetized (with plasma $\beta \simeq 0.1 - 0.01$) and rarefied (with densities two orders of magnitude lower than disk midplane densities) corona above ~ 2 scale heights is evident. Within both the disk and the corona, the “toroidal” component of the field (B_y), favored by differential rotation, dominates the poloidal component of the field by more than one order of magnitude (with $B_x^2 \simeq B_z^2$).

We can compare the predictions of our study to the mode structure that one might expect from the standard compressible MRI for the particular values of sound and Alfvén speeds found in the strongly magnetized corona by Miller & Stone (2000). In dimensionless units, $c_s = 0.007$ and, assuming a value of $\beta = 2(c_s/v_{A\phi})^2 \simeq 0.01$ and a toroidal-dominated magnetic field, yields $v_{A\phi} = 0.1$ and $v_{Az} = 0.01$. The largest features that their simulations are able to accommodate are those with $k \sim 60$ (corresponding to a wavelength of 10 in the vertical direction). As it can be seen in Figure 9, the role of the curvature terms is not negligible in two different respects. First, it completely stabilizes the perturbations on the longest scales well inside the numerical domain. Second, the growth rate for the unstable modes is significantly reduced.

It is difficult to extrapolate from the present work to address how the instabilities discussed here would couple to buoyancy in the presence of a stratified medium like the one considered by Miller & Stone (2000). A question, however, is raised about whether shearing boxes, because of their own Cartesian nature, constitute a good approach to simulating compressible flows in which superthermal toroidal fields are either imposed as initial field configurations or generated by shear.

6. SUMMARY AND CONCLUSIONS

In this paper we have addressed the role of toroidal fields on the stability of local axisymmetric perturbations in compressible, differentially rotating, MHD flows when the geometrical curvature of the background is taken into account. In order to accomplish this task, without imposing restrictions on the strength of the background equilibrium field, we relaxed the Boussinesq approximation. In particular, we have studied under which circumstances the curvature terms, intimately linked to magnetic tension in cylindrical coordinate systems, cannot be neglected. We have shown that the MRI is stabilized and two distinct instabilities appear for strong toroidal fields. At least for large wavenumbers, the structure of the modes seems to be the result of a purely local effect that is accounted for when compressibility and curvature terms are consistently taken into account. In particular we have demonstrated that, even for rotationally supported cylindrical flows, i.e., for $v_{A\phi} < 1$, both curvature terms and flow compressibility have to be considered if the toroidal Alfvén speed exceeds $\simeq \sqrt{\kappa c_s}$. This is true provided that the vertical Alfvén speed is not too large to invalidate the local limit.

There is little doubt that a realistic treatment of normal modes in magnetized accretion disks has to contemplate gradients in the flow variables over large scales and should, therefore, be global in nature. The results presented in this paper, however, provide the complete dispersion relation and, more importantly, analytic expressions for some of its solutions that should be recovered, in the appropriate limit, by a study of global modes in magnetized accretion disks, where compressibility effects are likely to be non negligible. We will address these issues in a future paper.

APPENDIX

Along the various sections of the present study, we have seen that the toroidal component of the magnetic field *does* play a role in the stability criterion and can in fact dominate the values of the critical wavenumber for superthermal fields and quasi toroidal configurations. A particular simple case in which the importance of considering both compressibility and magnetic tension terms can be appreciated is the study of modes with negligible frequency $\omega \ll 1$. We can obtain the wavenumber of these modes by imposing $\omega = 0$ to be a solution of the dispersion relation (23). We obtain, in physical dimensions,

$$k_o^2 = -2 \frac{d \ln \Omega}{d \ln r} \left(\frac{\Omega r}{v_{Az}} \right)^2 + 2\epsilon_1\epsilon_3 \left(\frac{v_{A\phi}}{v_{Az}} \right)^2 + \epsilon_2\epsilon_3 \left(\frac{v_{A\phi}}{v_{Az}} \right)^2 \left(\frac{v_{A\phi}}{c_s} \right)^2. \quad (49)$$

In what follows, let us consider a rotationally supported disk whose rotational profile is not too steep (i.e., $|d \ln \Omega / d \ln r|$ of order unity). The Alfvén speed v_{Az} appears in all three terms on the right hand side of equation (49) and therefore it does not play a role in determining the relative magnitudes between them. Unlike the second term, the third term is not necessarily small with respect to the first one, when superthermal fields are considered. In this case, we can note again (see §4.2) that it seems now safe to neglect the curvature term proportional to $\epsilon_1\delta B_\phi$ in equation (6). However, had we neglected the curvature term proportional to $\epsilon_2\delta\rho$ in equation (6) or the one proportional to $\epsilon_3\delta B_r$ in equation (7), we would have missed the important impact that the third term in equation (49) has on the stability of modes with $\omega \rightarrow 0$, in the limit of strong toroidal fields (see Fig. 3). This is somewhat counterintuitive because there does not seem to be any *a priori* indication about which of the magnetic tension terms (related to the curvature of the adopted coordinate system) is less relevant in the original set of equations (5)-(12) for the perturbations. This particular example illustrates the risks associated with neglecting terms that are not strictly 2nd order in the perturbed quantities but rather address the geometrical background in which the (local) analysis is being carried out.

From equation (49) it is also straightforward to see under which circumstances it is safe to neglect the curvature terms. For subthermal fields, k_o will not differ significantly from k_{BH} (eq. [25]) regardless of the geometry of the field configuration. This is because, if the field is weak enough ($v_A \ll c_s$), no matter how strong of a (subthermal) B_ϕ component we consider, the second and third term are negligible with respect to the first one. We conclude this short analysis by commenting that, while a strong vertical field plays a stabilizing role, in the sense that it drives k_o toward small values leaving all modes with shorter wavelengths stable, the consequences of considering strong toroidal fields is a little more subtle as it can be seen in the evolution of the structure of the modes in Figure 1.

We thank Eliot Quataert, Charles Gammie, and Wolfgang Duschl for useful discussion in different stages of this study. We also thank the Institute for Advanced Study for their hospitality during part of this investigation. This work was supported in part by NASA ATP grant.

REFERENCES

Balbus, S. A. 2003, *ARA & A*, 41, 555

Balbus, S. A., & Hawley, J. F. 1991, *ApJ*, 376, 214

———. 1992, *ApJ*, 392, 662

———. 1998, *Rev. Mod. Phys.*, 70, 1

———. 2002, *ApJ*, 573, 749

Blaes, O. M., & Balbus, S. A. 1994, *ApJ*, 421, 163

Bourke, T. L., & Goodman, A. A. 2003, In *Star Formation at High Angular Resolution*, ASP Conf. Ser., Vol. S-221, eds. M. G. Burton, R. Jayawardhana, and T. L. Bourke (astro-ph/0401281)

Curry, C., & Pudritz, R. E. 1995, *ApJ*, 453, 697

Dubrulle, B., & Knobloch, E. 1993, *A&A*, 274, 667

Gammie, C. F., & Balbus, S. A. 1994, *MNRAS*, 270, 138

Hawley, J. F., Gammie, C. F., & Balbus, S. A. 1994, in *ASP Conf. Ser. 54, The First Stromlo Symposium: The Physics of Active Galaxies*. ed. G. V. Bicknell, M. A. Dopita, & P.J. Quinn (San Francisco:ASP), 53

———. 1995, *ApJ*, 440, 742

———. 1996, *ApJ*, 464, 690

Knobloch, E. 1992, *MNRAS*, 255, 25

Kudoh, T., Matsumoto, R., & Shibata, K. 2002, *PASJ*, 54, 121

Machida, M., Hayashi, M. R., & Matsumoto R. 2000, *ApJ*, 532, L67

Miller, K. A., & Stone, J. M. 2000, *ApJ*, 534, 398

Myers, P. C., & Goodman A. A. 1988, *ApJ*, 326, L27

Ostriker, E. C., Stone, J. M., & Gammie, C. F. 2001, *ApJ*, 577, 524

Pariev, V. I., Blackman, E. G., & Boldyrev, S. A. 2003, *A&A*, 407, 403

Papaloizou J., & Szuszkiewicz E. 1992, *Geophys. Astrophys. Fluid Dyn.*, 66, 223

Press, W. H., Flannery, B. P., Teukolsky, S. A., & Vetterling, W. T. 1992, *Numerical Recipes* (Cambridge: University Press)

Pringle, J. E., 1989, *MNRAS*, 236, 107

Quataert, E., Dorland, W., & Hammet, G. W. 2002, *ApJ*, 577, 524

Sano, T., & Miyama, S. M. 1999, *ApJ*, 515, 776

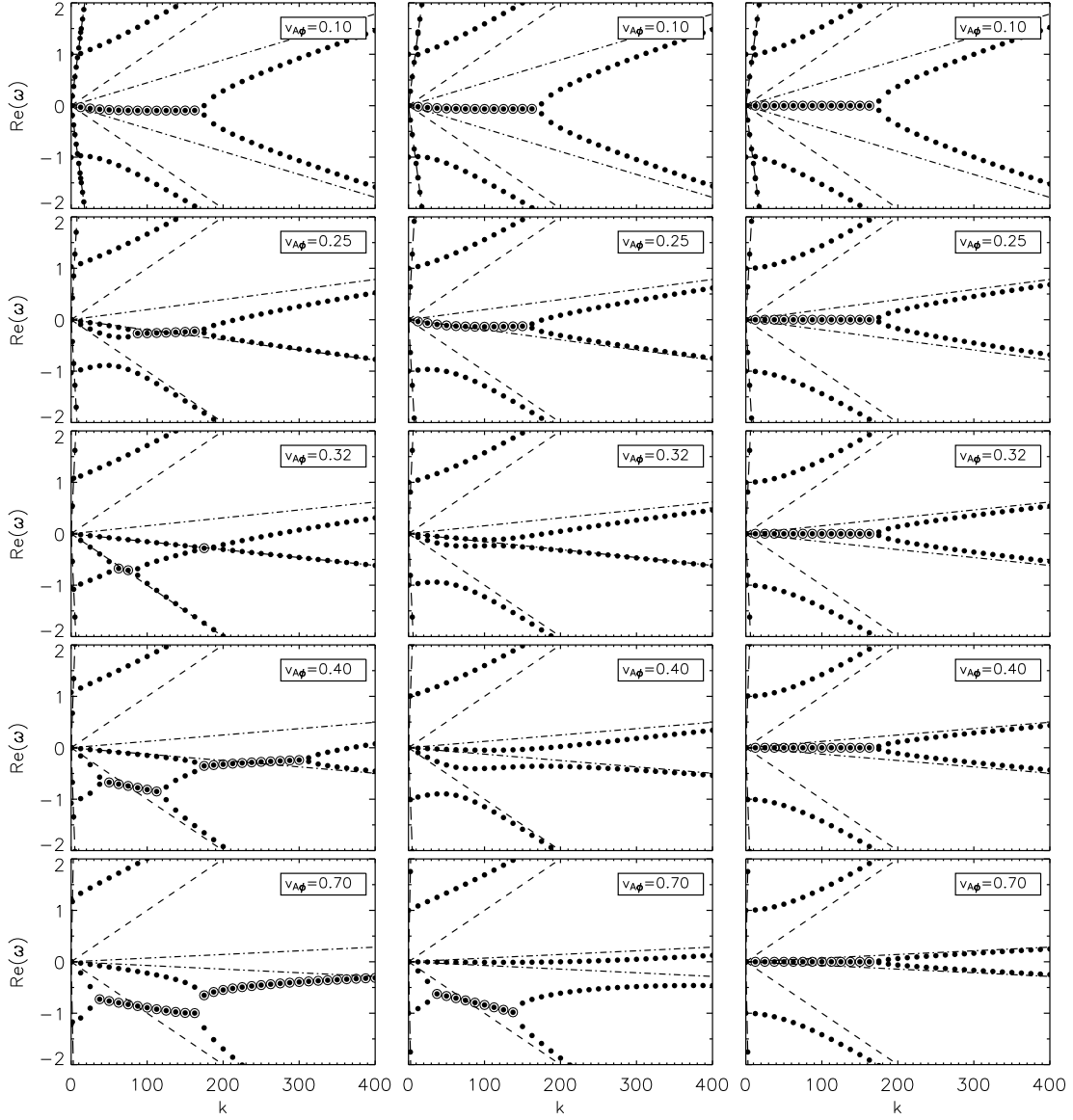


Fig. 1.— The real parts of the numerical solutions to the dispersion relation (23) corresponding to a Keplerian disk with $c_s = 0.05$ and $v_{Az} = 0.01$. *Left panel*: solutions to the full problem ($\epsilon_1 = \epsilon_2 = \epsilon_3 = \epsilon_4 = 1$). *Central panel*: the case in which compressibility is neglected in the curvature terms ($\epsilon_1 = \epsilon_3 = \epsilon_4 = 1$ and $\epsilon_2 = 0$). *Right panel*: the case in which all curvature terms are neglected ($\epsilon_1 = \epsilon_2 = \epsilon_3 = \epsilon_4 = 0$). Open circles indicate unstable modes (i.e., those with positive imaginary part). Long-dashed, short-dashed and point-dashed lines show the fast, Alfvén, and slow modes, respectively, in the limit of no rotation. Note that even for the highest value of the toroidal Alfvén speed considered here, the flow is still rotationally supported since, in that case, $B_\phi^2/8\pi\rho(r\Omega)^2 \simeq 0.25$.

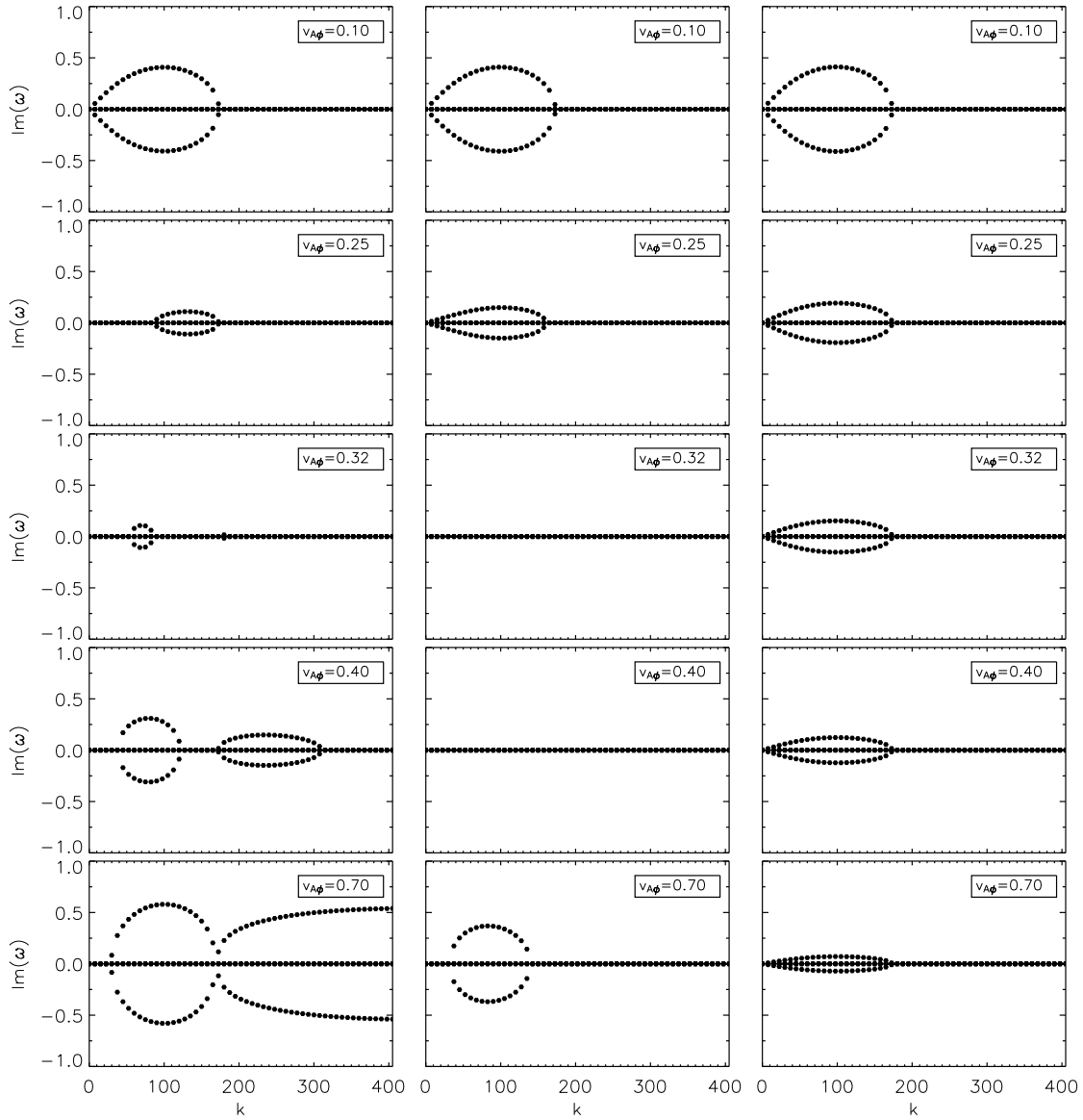


Fig. 2.— The imaginary parts for the cases discussed in Figure 1.

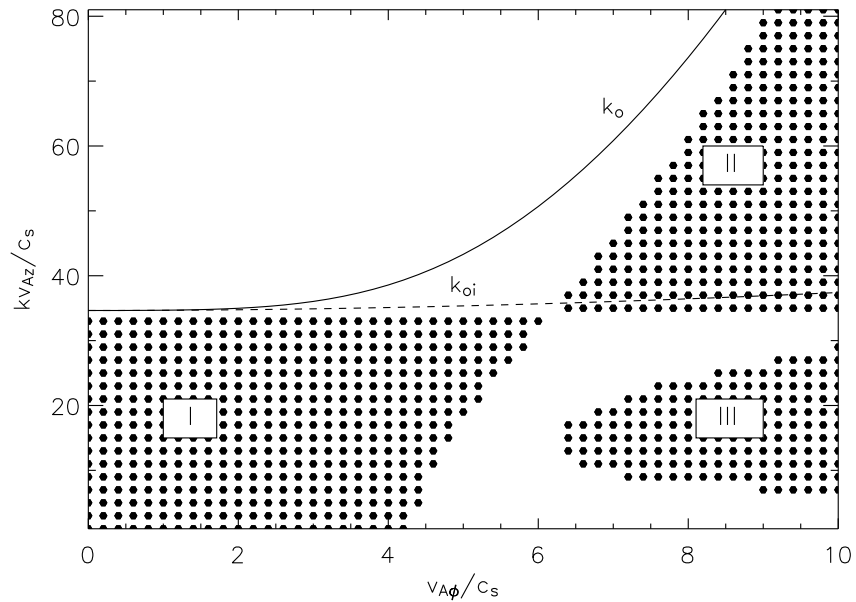


Fig. 3.— The black dots represent unstable modes obtained from solving the dispersion relation (23) numerically for a Keplerian disk with $c_s = 0.05$ and $v_{Az} = 0.01$. The solid (k_o) and dashed (k_{oi}) lines correspond to the variation of the critical wavenumber for which the $\omega = 0$ mode exists in the case of a compressible (see the Appendix) and an incompressible (discussed in §2) flow respectively. For strong toroidal fields, compressibility plays a crucial role in the stability of the $\omega = 0$ mode. Note that, in the limit of small $v_{A\phi}/c_s$ both, $k_o, k_{oi} \rightarrow k_{BH}$, and the trivial mode becomes unstable.

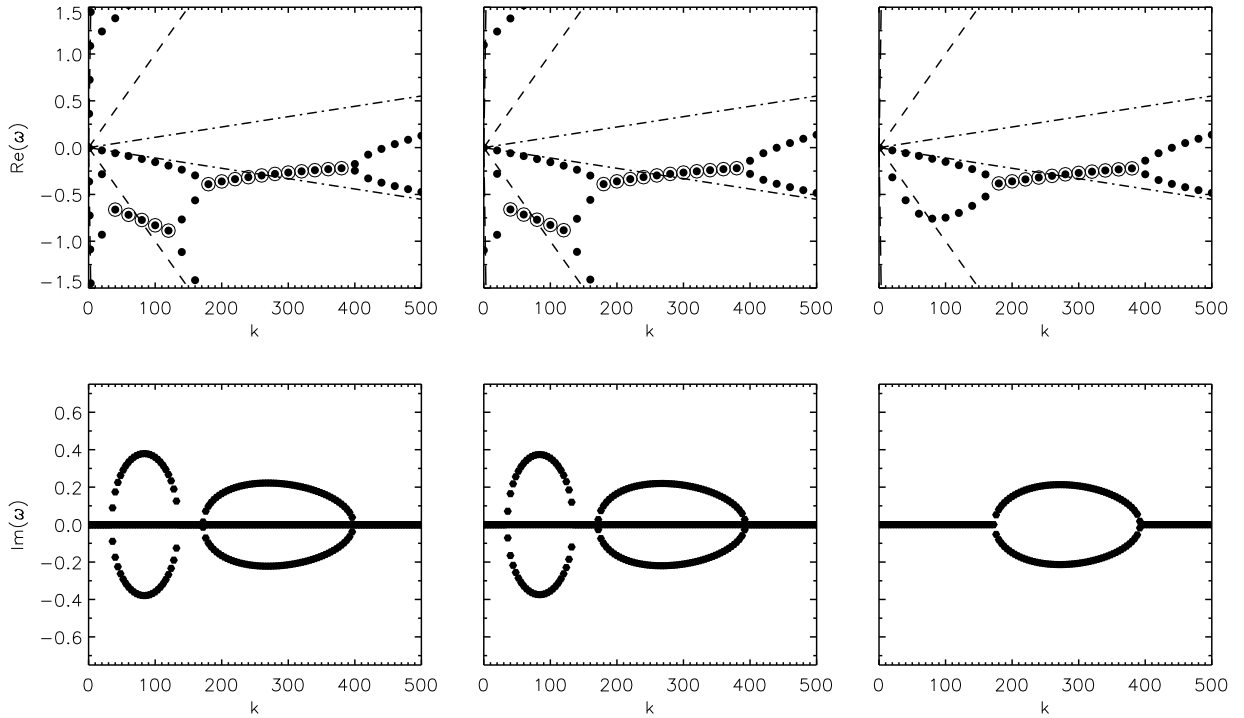


Fig. 4.— *Left panels*: Solutions to the full dispersion relation (23). *Central panels*: Solutions to the 4th order, approximate dispersion relation (36), with $\epsilon_2 = \epsilon_3 = \epsilon_4 = 1$. *Right panels*: Solutions to the 2nd order, approximate dispersion (39), with $\epsilon_2 = \epsilon_3 = 1$ and $\epsilon_4 = 0$. All solutions correspond to a Keplerian disk with $v_{A\phi} = 0.45$, $c_s = 0.05$, and $v_{Az} = 0.01$. Open circles in upper panels indicate unstable modes. Note that the phase velocities of the two instabilities (seen in either the leftmost or central upper panels and corresponding to Region II and III in §4.1) are similar to the phase velocities, positive and negative respectively, of the slow mode (point-dashed line) in the limit of no rotation. The magnetosonic modes can barely be seen close to the left axis of the first plot.

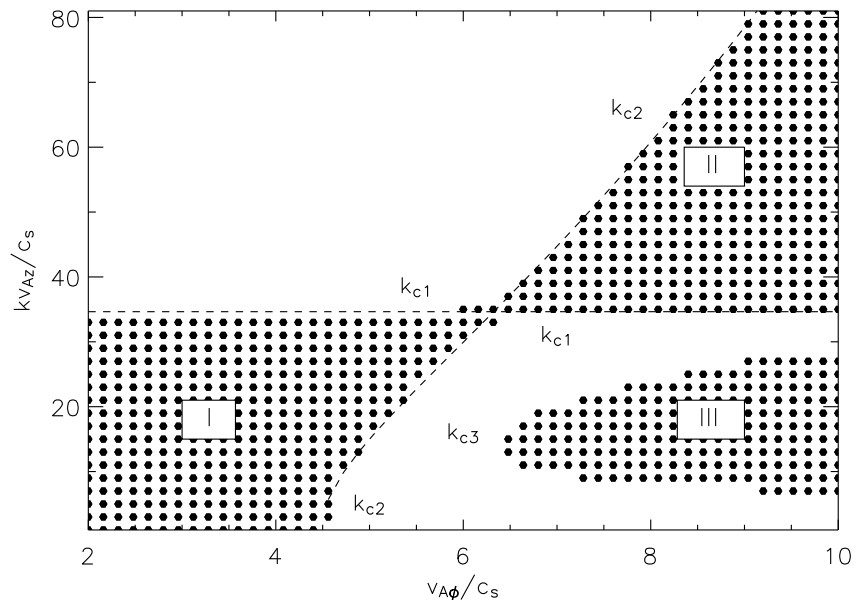


Fig. 5.— The black dots represent unstable modes satisfying the approximate instability criteria (38), described in §4.2. The dashed lines, labeled by k_{c1} and k_{c2} , are the limits of Regions I and II obtained analytically, also in §4.2. The onset of instability III is labeled by k_{c3} . As in Figure 3, a Keplerian disk with $c_s = 0.05$ and $v_{Az} = 0.01$, has been assumed.

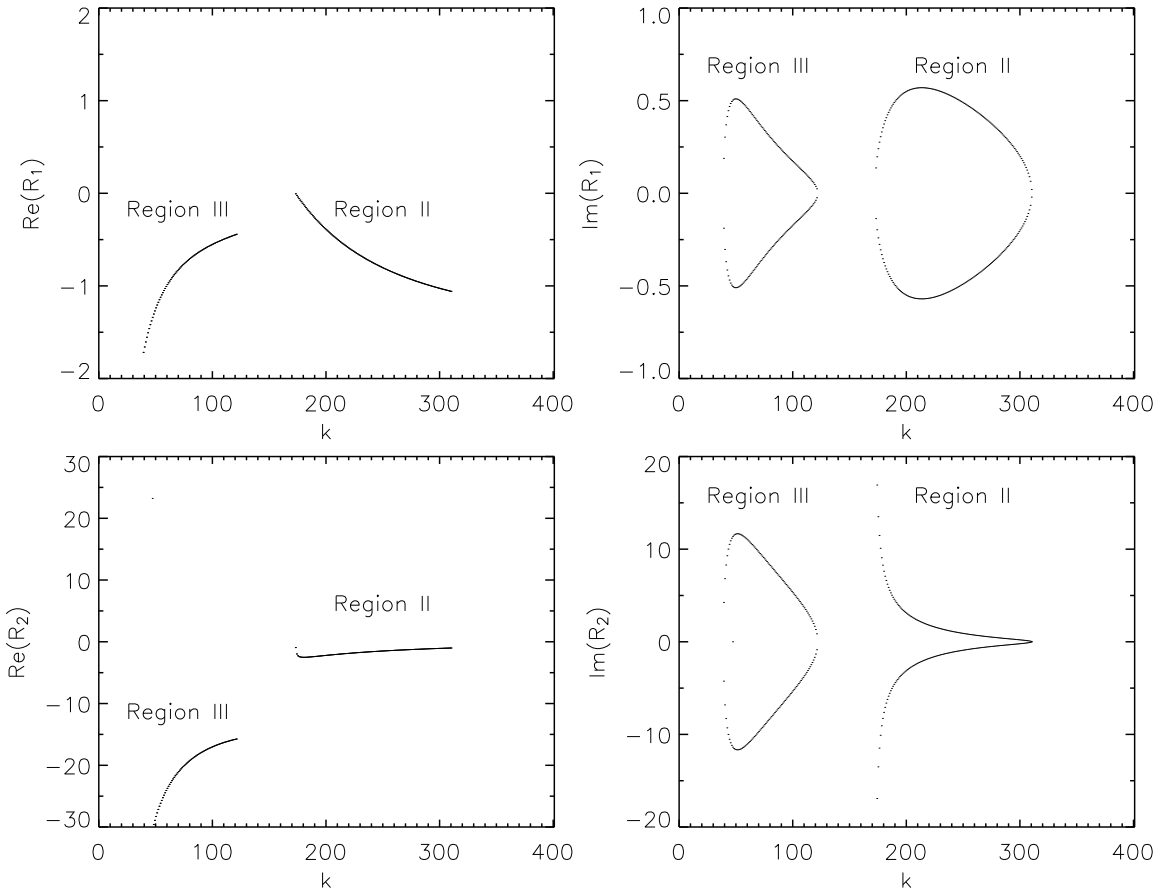


Fig. 6.— The importance of the curvature terms proportional to ϵ_2 and ϵ_3 , as defined by the ratios R_1 (eq. [47]) and R_2 (eq. [48]). For illustrative purposes, we have considered a Keplerian disk with $c_s = 0.05$, $v_{Az} = 0.01$, and $v_{A\phi} = 0.4$. Neither of these ratios (their real or imaginary parts) are negligible compared to unity. It is, therefore, not surprising that the curvature terms play an important role in determining the stability criteria of the MHD flow, when strong toroidal fields are present.

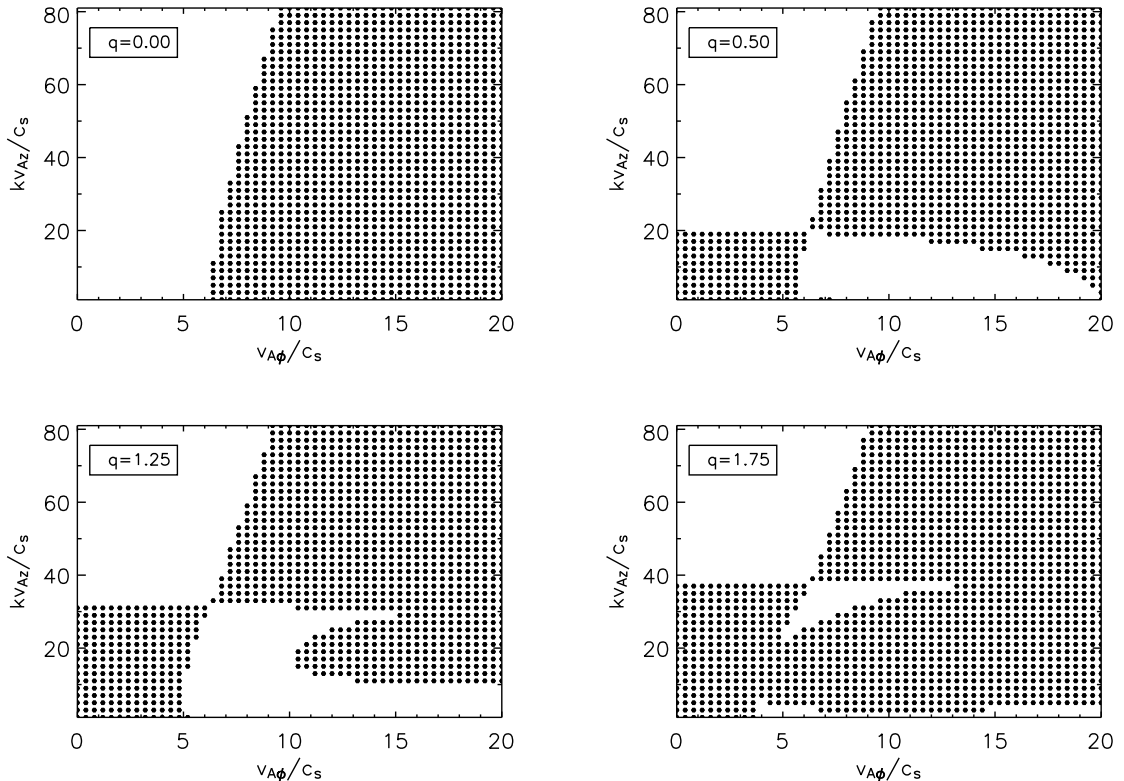


Fig. 7.— The black dots represent unstable modes obtained from solving numerically the dispersion relation (23) as a function of the toroidal Alfvén speed. As an example, we have assumed $c_s = 0.05$ and $v_{Az} = 0.01$. In each plot, different values of the rotational profile, $q = |d \ln \Omega / d \ln r|$, are considered. Note that, the highest value of the toroidal Alfvén speed considered here corresponds to the circular velocity.

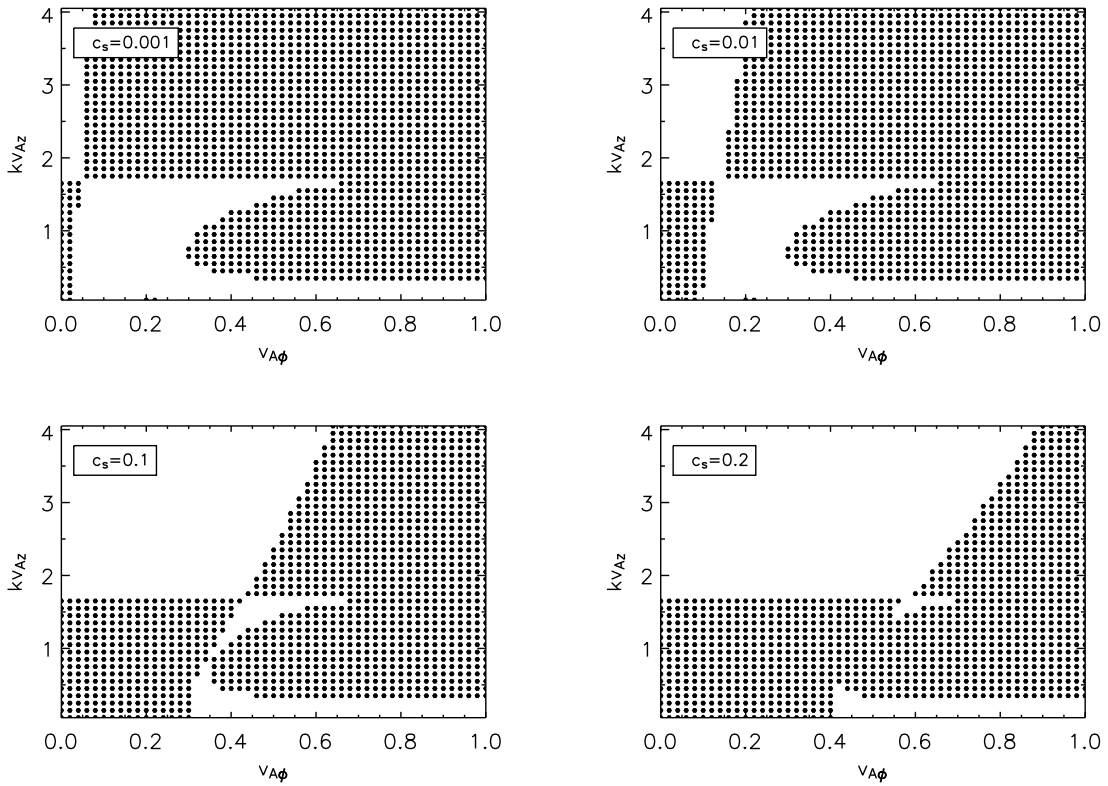


Fig. 8.— The black dots represent unstable modes obtained from solving the dispersion relation (23) numerically for a Keplerian disk with $v_{Az} = 0.01$. In each plot, different values of the local sound speed, c_s , are considered. Note that in this case, the axis are not normalized by the particular value of the local sound speed, but rather by our initial choice, see §2, of dimensionless variables.

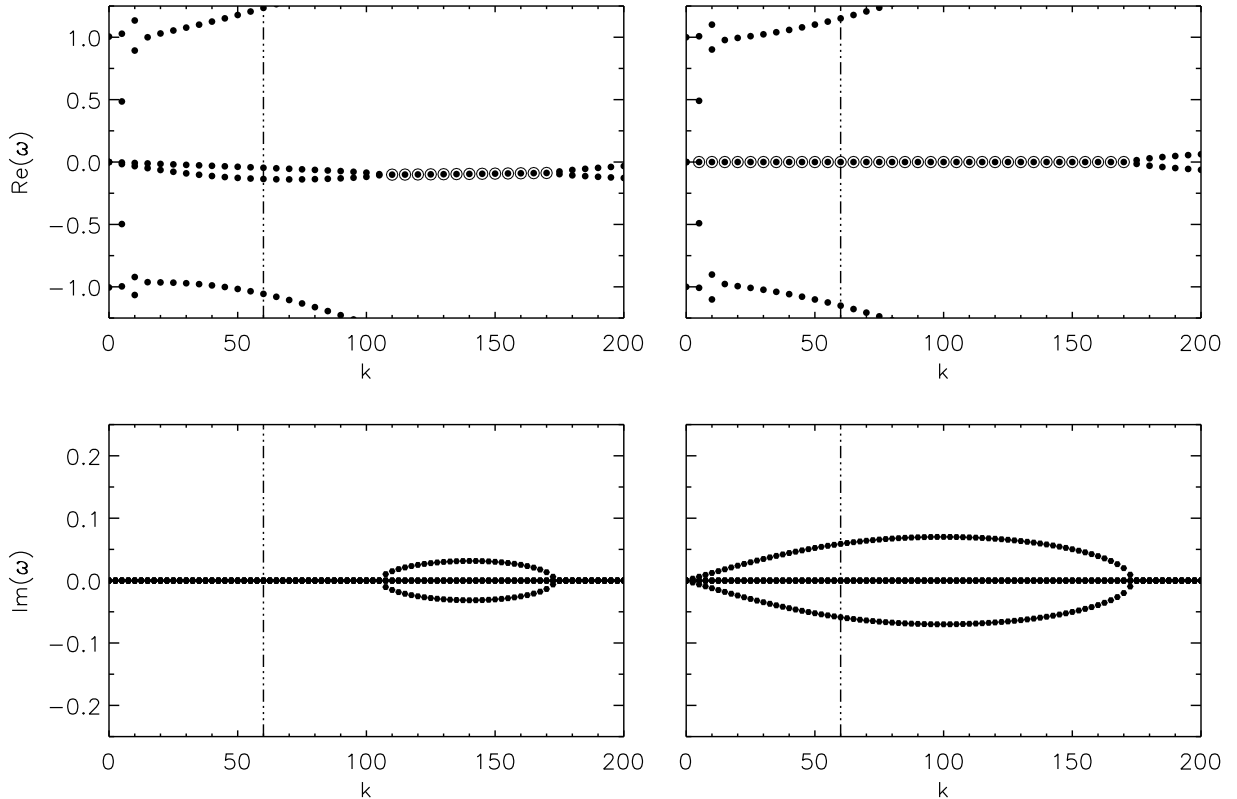


Fig. 9.— The implication of our study for shearing box simulations. *Left panels*: Solutions to the full dispersion relation (23), when all curvature terms are taken into account. *Right panels*: Solutions to the dispersion relation (24), i.e., when all curvature terms are neglected. In both cases, we have considered a Keplerian disk with $v_{A\phi} = 0.1$, $c_s = 0.007$, and $v_{Az} = 0.01$. Open circles in upper panels indicate unstable modes. The vertical line indicates the minimum wavenumber (i.e., largest wavelength) that can be accommodated in the simulations of a strongly-magnetized corona above a weakly magnetized disk by Miller & Stone (2000).